ERCOFTAC Workshop ASTROFLU V, Ecole Centrale, Lyon, France, 7-8 December 2021

Passive scalar fluctuations in turbulent flows simulation in the framework of the PITM method

Bruno Chaouat, ONERA, Université Paris-Saclay, France

Collaborations

Christophe Peyret, ONERA, Université Paris-Saclay, France

Roland Schiestel, IRPHE/CNRS, France

OUTLINE

- **Heat transfers are often involved in practical engineering and geophysical flows**
- **Motivation is to reproduce the *RMS* fluctuations of the scalar field that may have consequences in practical and geophysical flows**
- **The partially integrated transport modeling (PITM) method viewed as non-zonal hybrid RANS/LES performed on relatively coarse grids has been selected**
  - **Modeling is made in the spectral space for analyzing the physics of heat transfer**
  - **Equations of the half scalar variance k_θ and its dissipation rate ϵ_θ have been then extended to physical space**
- **Applications**
  - **Plane channel heated on both walls with a constant heat flux**
- **Numerical simulations are performed on several meshes for different Prandtl numbers $P_r = 0.1, 1$ and 10 at the Reynolds number $R_\tau = 395$**

1. IMPORTANCE OF THE PASSIVE SCALAR

- **Engineering applications in industrial plants**
- **In nature like for instance the pollution dispersal in atmosphere**
- **Variation of the scalar fields are supposed to have negligible action on the fluid movement**
- **PITM hybrid RANS/LES method solving the large turbulence and thermal scales is an efficient tool in practice for reducing the computational resources in comparison with highly resolved LES**

2. MATHEMATICAL FRAMEWORK OF PITM

- **Two-point velocity fluctuating correlation for non-homogeneous turbulence** $R_{ij} = \left\langle u'_{iA} u'_{jB} \right\rangle (\boldsymbol{x}_A, \boldsymbol{x}_B)$ **(Hinze, 1975)**
- **New independent variables**
  - **vector difference** $\boldsymbol{\xi} = \boldsymbol{x}_B - \boldsymbol{x}_A$
  - **midway position** $\boldsymbol{X} = \frac{1}{2}(\boldsymbol{x}_A + \boldsymbol{x}_B)$
- **Two-point fluctuating velocity correlation for non-homogeneous turbulence** $R_{ij} = \left\langle u'_{iA} u'_{jB} \right\rangle (\boldsymbol{X}, \boldsymbol{\xi})$
- **Taylor series development for the mean velocity (framework of tangent homogeneous spectral space , Schiestel, 1987; Chaouat and Schiestel, 2007)**
- **Fourier transform of the transport equation for the tensor** $R_{ij} = \left\langle u'_{iA} u'_{jB} \right\rangle$
- **Integration on a spherical shell in the wave numbers (Schiestel, 1987; Cambon et al., 1992; Chaouat and Schiestel, 2007)**

$$\varphi_{ij}(\kappa, \boldsymbol{X}) = (R_{ij}(\boldsymbol{X}, \boldsymbol{\xi}))^{\Delta} = \frac{1}{A(\kappa)} \iint_{\partial A} \widehat{R_{ij}}(\boldsymbol{\kappa}, \boldsymbol{X}) dA(\boldsymbol{\kappa}) \qquad \textbf{(1)}$$

3. EQUATION FOR THE TWO-POINT VELOCITY TENSOR

- **Equation of the spherical mean of the Fourier transform of the two-point correlation tensor of the fluctuating velocities $\varphi_{ij}(\boldsymbol{X}, \kappa, t)$ (Chaouat and Schiestel, 2005; 2007; 2013)**

$$\begin{aligned} \frac{\partial \varphi_{ij}(\boldsymbol{X},\kappa,t)}{\partial t} + \langle u_j \rangle (\boldsymbol{X}) \frac{\partial \varphi_{ij}(\boldsymbol{X},\kappa,t)}{\partial X_j} \quad &= \quad \mathcal{P}_{ij}(\boldsymbol{X},\kappa,t) + \mathcal{T}_{ij}(\boldsymbol{X},\kappa,t) \\ +\Psi_{ij}(\boldsymbol{X},\kappa,t) + \mathcal{J}_{ij}(\boldsymbol{X},\kappa,t) - \mathcal{E}_{ij}(\boldsymbol{X},\kappa,t) & \end{aligned} \tag{2}$$

where $\mathcal{P}_{ij}$, $\mathcal{T}_{ij}$, Ψ_{ij}, $\mathcal{J}_{ij}$, and $\mathcal{E}_{ij}$ are respectively, the production, transfer, redistribution, diffusion and dissipation terms.

4. TRANSPORT EQUATIONS

As a result (Chaouat and Schiestel, 2005, 2009, 2012), the transport equation for the subfilter scale stress (SFS) tensor $(\tau_{ij})_{sfs}$ can be written in the simple compact form as

$$\frac{\partial(\tau_{ij})_{sfs}}{\partial t} + \frac{\partial}{\partial x_k}(\bar{u}_k(\tau_{ij})_{sfs}) = (P_{ij})_{sfs} + (\Pi_{ij})_{sfs} - \epsilon_{ij} + (J_{ij})_{sfs} \qquad (3)$$

where the terms appearing in the right-hand side of this equation are identified as subfilter production, redistribution and dissipation turbulent diffusion, respectively, while the transport equation for the dissipation rate ϵ reads

$$\frac{\partial \epsilon}{\partial t} + \frac{\partial}{\partial x_k}(\bar{u}_k \epsilon) = c_{\epsilon_{1sfs}} \frac{\epsilon}{k_{sfs}} P_{sfs} - c_{\epsilon_{2sfs}} \frac{\epsilon^2}{k_{sfs}} + J_{\epsilon sfs} \qquad (4)$$

The coefficient appearing in the destruction term of Equation (4) is a dynamical coefficient.

5. Calibration of the dynamical coefficient

The dynamical coefficient is given by

$$c_{\epsilon_{2sfs}} = c_{\epsilon_1} + \frac{k_{sfs}}{k}\Delta c_\epsilon \tag{5}$$

where $\Delta c_\epsilon = c_{\epsilon_2} - c_{\epsilon_1}$, c_{ϵ_1} and c_{ϵ_2} are the coefficients used in RANS. Using the energy density spectrum defined as $E(\kappa) = kLE^*(\vartheta)$, where L denotes the turbulence length-scale $L = k^{3/2}/\epsilon$, $\vartheta = \kappa L$,

$$E^*(\vartheta) = \frac{\frac{2}{3}\beta\vartheta^{\alpha-1}}{[1+\beta\vartheta^\alpha]^{\gamma+1}} \tag{6}$$

One can obtain after integration (Chaouat and Schiestel, 2005)

$$c_{\epsilon_{2sfs}}(\vartheta_c) = c_{\epsilon_1} + \frac{\Delta c_\epsilon}{[1+\beta\vartheta_c^\alpha]^\gamma} \tag{7}$$

where $\alpha\gamma = 2/3$ and $\beta = [2/(3C_K)]^\gamma$, C_K is the Kolmogorov constant close to 1.5, $\vartheta_c = \kappa_c L$

6. PITM FOR THE PASSIVE SCALAR

- **Two-point fluctuating scalar correlation for non-homogeneous turbulence** $\phi_{ij} = \langle \theta'_{iA} \theta_{jB} \rangle (\boldsymbol{x}_A, \boldsymbol{x}_B)$ **(Hinze, 1975, Chaouat and Schiestel, 2021)**
- **New independent variables**
  - **vector difference** $\boldsymbol{\xi} = \boldsymbol{x}_B - \boldsymbol{x}_A$
  - **midway position** $\boldsymbol{X} = \frac{1}{2}(\boldsymbol{x}_A + \boldsymbol{x}_B)$
- **Taylor series development for the mean velocity (framework of tangent homogeneous spectral space, Schiestel, 1987; Chaouat and Schiestel, 2007)**
- **Fourier transform of the transport equation for the tensor** $\phi_{\theta\theta} = \langle \theta'_A \theta'_B \rangle$
- **Integration on a spherical shell in the wave numbers (Schiestel, 1987; Cambon et al., 1992; Chaouat and Schiestel, 2007, Chaouat and Schiestel, 2021)**

$$\varphi_{\theta\theta}(\kappa, \boldsymbol{X}) = (\phi_{\theta\theta}(\boldsymbol{X}, \boldsymbol{\xi}))^{\Delta} = \frac{1}{A(\kappa)} \iint_{\partial A} \widehat{\phi_{\theta\theta}}(\boldsymbol{\kappa}, \boldsymbol{X}) dA(\boldsymbol{\kappa}) \qquad \textbf{(8)}$$

7. EQUATION FOR THE SCALAR VARIANCE

- **The spectral transport equation of half the scalar variance denoted as $E_\theta = \varphi_{\theta\theta}/2$ (Chaouat and Schiestel, 2021)**

$$\frac{\partial E_\theta(\boldsymbol{X},\kappa)}{\partial t} + \langle u_k \rangle (\boldsymbol{X}) \frac{\partial E_\theta(\boldsymbol{X},\kappa)}{\partial X_k} = \mathcal{P}_\theta(\boldsymbol{X},\kappa) + \mathcal{T}_\theta(\boldsymbol{X},\kappa) + \mathcal{J}_\theta(\boldsymbol{X},\kappa) - \mathcal{E}_\theta(\boldsymbol{X},\kappa) \tag{9}$$

where in the right hand side of this equation, $\mathcal{P}_\theta$ is the production of half the scalar variance by mean gradients of the scalar, $\mathcal{T}_\theta$ is the spectral transfer driven by the eddying motions in the inertial cascade, $\mathcal{J}_\theta$ is the diffusion term and $\mathcal{E}_\theta$ denotes the dissipation term of half the scalar variance. Homogeneous flows are considered in the following.

8. SPECTRAL ANALYTICAL EXPRESSIONS

- **Production** $\mathcal{P}_{\theta j}$

$$\mathcal{P}_\theta(\boldsymbol{X},\kappa,t) = -\varphi_{j\theta}(\boldsymbol{X},\kappa,t)\frac{\partial \langle\theta\rangle}{\partial X_j} \tag{10}$$

- **Transfer** $\mathcal{T}_\theta$

$$\mathcal{T}_\theta(\boldsymbol{X},\kappa,t) = -\frac{1}{2}\left(\xi_m \frac{\partial \phi_{\theta\theta}}{\partial \xi_j}(\boldsymbol{X},\boldsymbol{\xi},t)\right)^\Delta \frac{\partial \langle u_j\rangle}{\partial X_m} - \frac{1}{2}\left(\frac{\partial}{\partial \xi_j}(S_{\theta,j\theta} - S_{\theta j,\theta}(\boldsymbol{X},\boldsymbol{\xi},t))\right)^\Delta \tag{11}$$

- **Diffusion** $\mathcal{J}_\theta$

$$\mathcal{J}_\theta(\boldsymbol{X},\kappa,t) = -\frac{1}{4}\frac{\partial}{\partial X_j}\left(S^\Delta_{\theta,j\theta} + S^\Delta_{\theta j,\theta}\right) + \sigma \frac{\partial^2 E_\theta}{\partial X_j \partial X_j}(\boldsymbol{X},\boldsymbol{\xi},t) \tag{12}$$

- **Dissipation** $\mathcal{E}_\theta$

$$\mathcal{E}_\theta = \frac{\sigma}{2}\frac{\partial^2 E_\theta}{\partial X_j \partial X_j}(\boldsymbol{X},\boldsymbol{\xi},t) + 2\sigma\kappa^2 E_\theta(\boldsymbol{X},\boldsymbol{\xi},t) \tag{13}$$

9. INTEGRATION IN THE SPECTRAL SPACE

Equation (9) is integrated in the domains $[0, \kappa_c]$, $[\kappa_c, \kappa_e]$ and $[\kappa_e, \infty[$ where κ_e denotes here the high end wave number that is larger than κ_c and different from κ_d. Homogeneous flows are considered in the following.

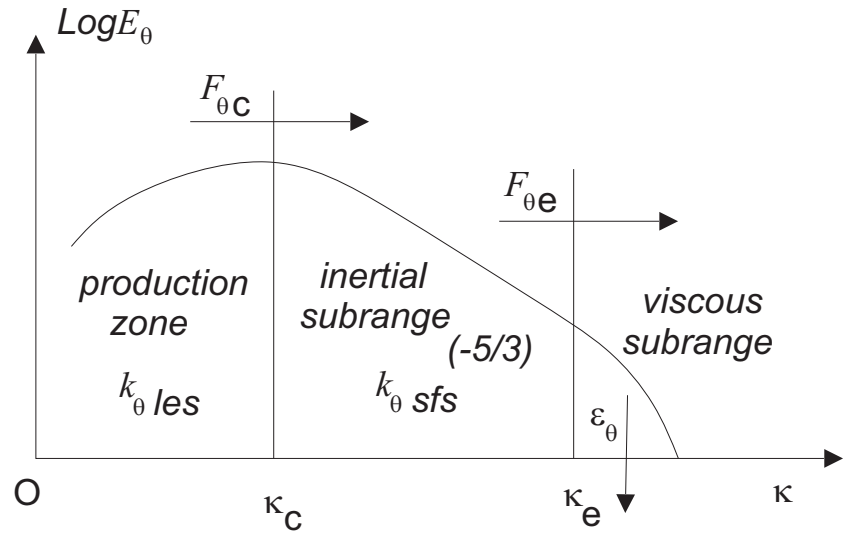

Figure 1: Sketch of spectral splitting of scalar variance

10. EQUATIONS

Integration of the spectral density equation (9) for $E_\theta(\boldsymbol{X}, \kappa)$ leads to the following equations :

$$\frac{\partial k_{\theta les}}{\partial t} = P_{\theta[0,\kappa_c]} - F_\theta(\kappa_c, t) \tag{14}$$

$$\frac{\partial k_{\theta sfs}}{\partial t} = P_{\theta[\kappa_c,\kappa_e]} - F_\theta(\kappa_e, t) + F_\theta(\kappa_c, t) \tag{15}$$

$$0 = F_\theta(\kappa_e, t) - \epsilon_{\theta[\kappa_e,\infty[} \tag{16}$$

where

$$k_{\theta sfs} = \int_{\kappa_c}^{\kappa_e} E_\theta(\kappa, t) d\kappa \quad , \quad k_{\theta les} = \int_0^{\kappa_c} E_\theta(\kappa, t) d\kappa \quad , \quad k_\theta = k_{\theta les} + k_{\theta sfs} \tag{17}$$

$$F_\theta(\kappa_c, t) = \mathcal{F}_\theta(\kappa_c, t) - E_\theta(\kappa_c, t) \frac{\partial \kappa_c}{\partial t} \tag{18}$$

$$F_\theta(\kappa_e, t) = \mathcal{F}_\theta(\kappa_e, t) - E_\theta(\kappa_e, t) \frac{\partial \kappa_e}{\partial t} \tag{19}$$

and

$$\epsilon_{\theta[\kappa_e,\infty]} = \int_{\kappa_e}^{\infty} \mathcal{E}_\theta(\kappa, t) d\kappa \tag{20}$$

where $\epsilon_{\theta[\kappa_e,\infty]} \approx \epsilon_\theta$**.**

11. BASIC CALCULUS

Eq. (15) can be then rewritten as

$$\frac{\partial k_{\theta\, sfs}}{\partial t} = P_{\theta[\kappa_c,\kappa_e]} + F_\theta(\kappa_c, t) - \epsilon_\theta \tag{21}$$

The relation $\kappa_e - \kappa_c = \mathcal{O}(1/l_\theta) = \mathcal{O}(\epsilon_\theta/\theta^2 u)$ **leads to the equation**

$$\kappa_e - \kappa_c = \zeta_\theta \frac{\epsilon_\theta}{k_{\theta\, s} k_s^{1/2}} \tag{22}$$

where ζ_θ **is an adjustable coefficient chosen such that the spectral contribution of the variance beyond** κ_e **is negligible. Combining these equations together yields**

$$\frac{\partial \epsilon_\theta}{\partial t} = \frac{\epsilon_\theta}{k_{\theta\, sfs}} \frac{\partial k_{\theta\, sfs}}{\partial t} + \frac{\epsilon_\theta}{2k_{sfs}} \frac{\partial k_{sfs}}{\partial t} + \frac{\epsilon_\theta}{\kappa_e - \kappa_c} \left[\frac{\mathcal{F}_\theta(\kappa_e, t) - F_\theta(\kappa_e, t)}{E_\theta(\kappa_e, t)} - \frac{\mathcal{F}_\theta(\kappa_c, t) - F_\theta(\kappa_c, t)}{E_\theta(\kappa_c, t)} \right] \tag{23}$$

12. TRANSPORT EQUATION FOR THE DISSIPATION

Using the transport equations for k_{sfs} and ϵ (Chaouat and Schiestel, 2005), one can obtain easily the resulting equation for the dissipation-rate ϵ_θ written in a more compact form as

$$\frac{\partial \epsilon_\theta}{\partial t} = c_{\epsilon\theta\theta_1 sfs} P_{\theta sfs} \frac{\epsilon_\theta}{k_{\theta sfs}} + c_{\epsilon\theta k_1 sfs} P_{sfs} \frac{\epsilon_\theta}{k_{sfs}} - c_{\epsilon\theta k_2 sfs} \frac{\epsilon_\theta \epsilon}{k_{sfs}} - c_{\epsilon\theta\theta_2 sfs} \frac{\epsilon_\theta^2}{k_{\theta sfs}} \tag{24}$$

where

$$P_{\theta sfs} = P_{\theta[\kappa_c,\kappa_e]} + F_\theta(\kappa_c) \tag{25}$$

$$c_{\epsilon\theta\theta_1 sfs} = 1 \quad , \quad c_{\epsilon\theta k_1 sfs} = \frac{1}{2} \quad , \quad c_{\epsilon\theta k_2 sfs} = \frac{1}{2} \tag{26}$$

and

$$c_{\epsilon\theta\theta_2 sfs} = 1 - \frac{k_{\theta sfs}}{(\kappa_e - \kappa_c) E_\theta(\kappa_e)} \left[\left(\frac{\mathcal{F}_\theta(\kappa_e) - F_\theta(\kappa_e)}{\epsilon_\theta} \right) - \frac{E_\theta(\kappa_e)}{E_\theta(\kappa_c)} \frac{F_\theta(\kappa_c)}{\epsilon_\theta} \left(\frac{\mathcal{F}_\theta(\kappa_c)}{F_\theta(\kappa_c)} - 1 \right) \right] \tag{27}$$

13. EXPRESSION OF THE DYNAMICAL COEFFICIENT

Setting $\kappa_c \ll \kappa_e$, $E(\kappa_d) \ll E(\kappa_c)$, and $E_\theta(\kappa_e) \ll E_\theta(\kappa_c)$, and also considering that $F_\theta(\kappa_e) = \epsilon_\theta$ as indicated by Eq. (16), Eq. (27) reduces then to

$$c_{\epsilon_{\theta\theta_2 sfs}} = 1 - \frac{k_{\theta sfs}}{\kappa_e E_\theta(\kappa_e)} \left(\frac{\mathcal{F}_\theta(\kappa_e)}{\epsilon_\theta} - 1 \right) \tag{28}$$

When κ_c goes to zero, that is to say when the filter width in physical space goes to infinity in an homogeneous turbulence field (or locally homogeneous),

$$c_{\epsilon_{\theta\theta_2}} = 1 - \frac{k_\theta}{\kappa_e E_\theta(\kappa_e)} \left(\frac{\mathcal{F}_\theta(\kappa_e)}{\epsilon_\theta} - 1 \right) \tag{29}$$

Comparing Eq. (28) with Eq. (29) leads to (Chaouat and Schiestel, 2021)

$$c_{\epsilon_{\theta\theta_2 sfs}} = c_{\epsilon_{\theta\theta_1}} + \frac{k_{\theta sfs}}{k_\theta} \left(c_{\epsilon_{\theta\theta_2}} - c_{\epsilon_{\theta\theta_1}} \right) \tag{30}$$

14. Molecular Prandtl numbers near unity

The ratio $k_{\theta\,sfs}/k_\theta$ must be calibrated as a function of the location of the cutoff wavenumber. The spectrum of the scalar in the equilibrium range can be approximated by

$$E_\theta(\kappa) = C_\theta \epsilon_\theta \epsilon^{-1/3} \kappa^{-5/3} \tag{31}$$

where C_θ is a constant coefficient close to 0.5. The spectrum of the scalar θ is extended in the whole range domain of the wavenumbers

$$E_\theta(\kappa) = \frac{C_\theta \epsilon_\theta}{C_K \epsilon} E(\kappa) \tag{32}$$

where $E(\kappa)$ is the energy density spectrum of turbulence. Equation (32) must verify the limiting condition $\lim_{\kappa\to\infty} E_\theta(\kappa) = C_\theta \epsilon_\theta \epsilon^{-1/3} \kappa^{-5/3}$. The analytical integration yields the practical result (Chaouat and Schiestel, 2021)

$$c_{\epsilon\theta\theta_{2}\,sfs}(\vartheta_c) = c_{\epsilon\theta\theta_1} + \frac{\Delta c_{\epsilon\theta\theta}}{[1+\beta\vartheta_c^{\alpha}]^{\gamma}} \tag{33}$$

where $\Delta c_{\epsilon\theta\theta} = c_{\epsilon\theta\theta_2} - c_{\epsilon\theta\theta_1}$.

15. Small Molecular Prandtl numbers

This situation corresponds to the case of liquid metals. The inertial subrange of the variance spectrum is shorter due to high molecular diffusivity

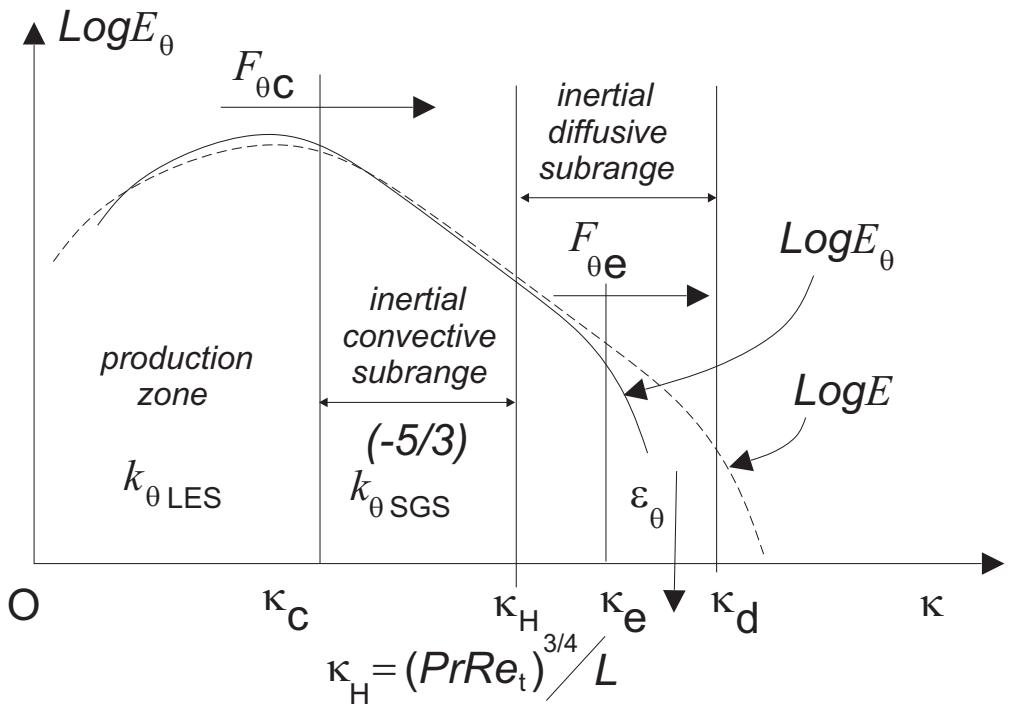

Figure 2: Spectral zones for small molecular Prandtl numbers where $\kappa_H = (\epsilon/\sigma^3)^{1/4}$ and $L = k^{3/2}/\epsilon$.

16. Small Molecular Prandtl numbers

The spectrum of the scalar variance is given by the function

$$E_\theta(\kappa) = C_\theta \epsilon_\theta \epsilon^{-1/3} \kappa^{-5/3} \exp\left[-\frac{3}{2} C_\theta (\kappa \eta_\theta)^{4/3}\right] \tag{34}$$

with the scalar microscale defined by $\eta_\theta = \left(\sigma^3/\epsilon\right)^{1/4} = (\nu^3/\epsilon)^{1/4}$ **where** $C_\theta = 1.5$**. In practice, Equation (34) is replaced by**

$$E_\theta(\kappa) = C_\theta \epsilon_\theta \epsilon^{-1/3} \kappa^{-5/3} H(\kappa_H - \kappa) \tag{35}$$

where $\kappa_H = 1/\eta_\theta$**, and** H **is the Heaviside function (** $E_\theta(\kappa) = 0$ **for** $\kappa \geq \kappa_H$**). The dimensionless variable** ϑ **is dropping for** $\vartheta_H = (P_r Re_t)^{3/4} = k^{3/2}/(\eta_\theta\, \epsilon)$ $Pe_t = P_r Re_t$**.** $c_{\epsilon\theta\theta_2 sfs}$ **is obtain by integrating the spectrum (35) leading to (Chaouat and Schiestel, 2021)**

$$c_{\epsilon\theta\theta_2 sfs}(\vartheta_c) = \begin{cases} c_{\epsilon\theta\theta_1} + \Delta c_{\epsilon\theta\theta} \dfrac{\left[1+\beta\vartheta_c^\alpha\right]^{-\gamma} - \left[1+\beta Pe_t^{3\alpha/4}\right]^{-\gamma}}{1 - \left[1+\beta Pe_t^{3\alpha/4}\right]^{-\gamma}} & (\vartheta_c < \vartheta_H) \\ c_{\epsilon\theta\theta_1} & (\vartheta_c > \vartheta_H) \end{cases} \tag{36}$$

17. Large Molecular Prandtl numbers

This situation corresponds to the case of poorly conducting fluids or high viscous fluids like most of oils. The inertial subrange is followed by a viscous-convective subrange and a viscous-diffusive subrange.

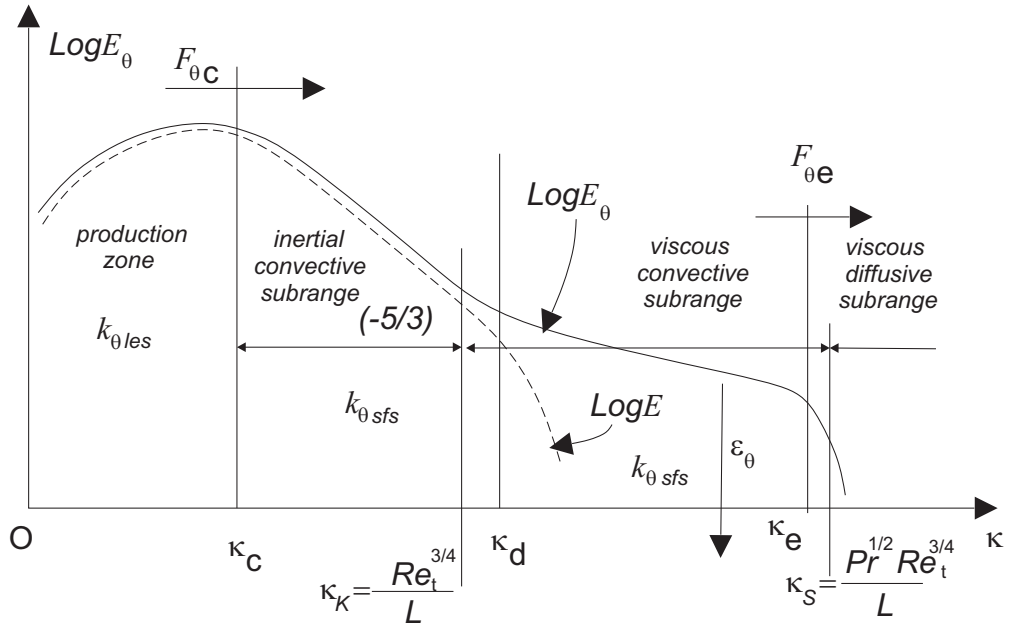

Figure 3: Spectral zones for large molecular Prandtl numbers where $\kappa_K = 1/\eta_K$ and $\kappa_S = P_r^{1/2}/\eta_K$ with $\eta_K = (\nu^3/\epsilon)^{1/4}$ and $L = k^{3/2}/\epsilon$.

18. Large Molecular Prandtl numbers

For the wave number $\kappa \geq 1/\eta_K$

$$E_\theta(\kappa) = c_\theta \epsilon_\theta \left(\frac{\nu}{\epsilon}\right)^{1/2} \kappa^{-1} \tag{37}$$

where c_θ **is a constant coefficient. The viscous convective subrange is followed by the viscous-diffusive subrange**

$$E_\theta(\kappa) = c_\theta \epsilon_\theta \left(\frac{\nu}{\epsilon}\right)^{1/2} \kappa^{-1} \exp\left[-c_\theta (\kappa \eta_\theta^*)^2\right] \tag{38}$$

where $\eta_\theta^* = \eta_K (\sigma/\nu)^{1/2} = \eta_K / \sqrt{P_r}$ **is the smallest scale of the viscous-diffusive subrange and** c_θ **is a constant coefficient. The corresponding wave numbers are then computed as** $\kappa_K = 1/\eta_K$ **and** $\kappa_S = 1/\eta_\theta^*$**. The junctions between the different curves occur for** $\kappa = \kappa_K$ **and** $\kappa = \kappa_S$**.** $\vartheta_K = Re_t^{3/4}$ **and** $\vartheta_S = P_r^{1/2} Re_t^{3/4}$**, respectively.**

19. Large Molecular Prandtl numbers

In practice, a simple approach is retained. The spectrum given by Equation (38) is replaced by a simple form as In the first wave number range $[0, \kappa_K]$, the spectrum $E_{\theta_1}(\kappa)$ is defined as

$$E_{\theta_1}(\kappa) = \xi \frac{k_\theta}{k} E(\kappa) \tag{39}$$

where $E(\kappa)$ is given by Equation (6) whereas in the second domain $[\kappa_K, \infty[$, the spectrum $E_{\theta_2}(\kappa)$ is

$$E_{\theta_2}(\kappa) = \xi c_\theta \epsilon_\theta \left(\frac{\nu}{\epsilon}\right)^{1/2} \kappa^{-1} H(\kappa_S - \kappa) \tag{40}$$

where ξ is a coefficient of normalization.

20. Large Molecular Prandtl numbers

Integration of the spectrum leads to three different values depending on the spectrum zones

(A) : $(\vartheta_C < \vartheta_K)$.

(B) : $(\vartheta_K < \vartheta_C < \vartheta_S)$.

(C) : $(\vartheta_S < \vartheta_C)$.

As a result (Chaouat and Schiestel, 2021)

$$c_{\epsilon\theta\theta_2 sfs}(\vartheta_c) = \begin{cases} c_{\epsilon\theta\theta_1} + \Delta c_{\epsilon\theta\theta} \dfrac{[1+\beta\vartheta_c^{\alpha}]^{-\gamma} - \left[1+\beta Re_t^{3\alpha/4}\right]^{-\gamma} + c_\theta \frac{\epsilon_\theta}{k_\theta}\left(\frac{\nu}{\epsilon}\right)^{1/2} \ln P_r^{1/2}}{1 - \left[1+\beta Re_t^{3\alpha/4}\right]^{-\gamma} + c_\theta \frac{\epsilon_\theta}{k_\theta}\left(\frac{\nu}{\epsilon}\right)^{1/2} \ln P_r^{1/2}} & (A) \\ c_{\epsilon\theta\theta_1} + \Delta c_{\epsilon\theta\theta} \dfrac{c_\theta \frac{\epsilon_\theta}{k_\theta}\left(\frac{\nu}{\epsilon}\right)^{1/2} \ln \frac{\vartheta_S}{\vartheta_c}}{1 - \left[1+\beta Re_t^{3\alpha/4}\right]^{-\gamma} + c_\theta \frac{\epsilon_\theta}{k_\theta}\left(\frac{\nu}{\epsilon}\right)^{1/2} \ln P_r^{1/2}} & (B) \\ c_{\epsilon\theta\theta_1} & (C) \end{cases}$$

21. Variation of the coefficient $C_{\epsilon\theta\theta_2 sfs}$

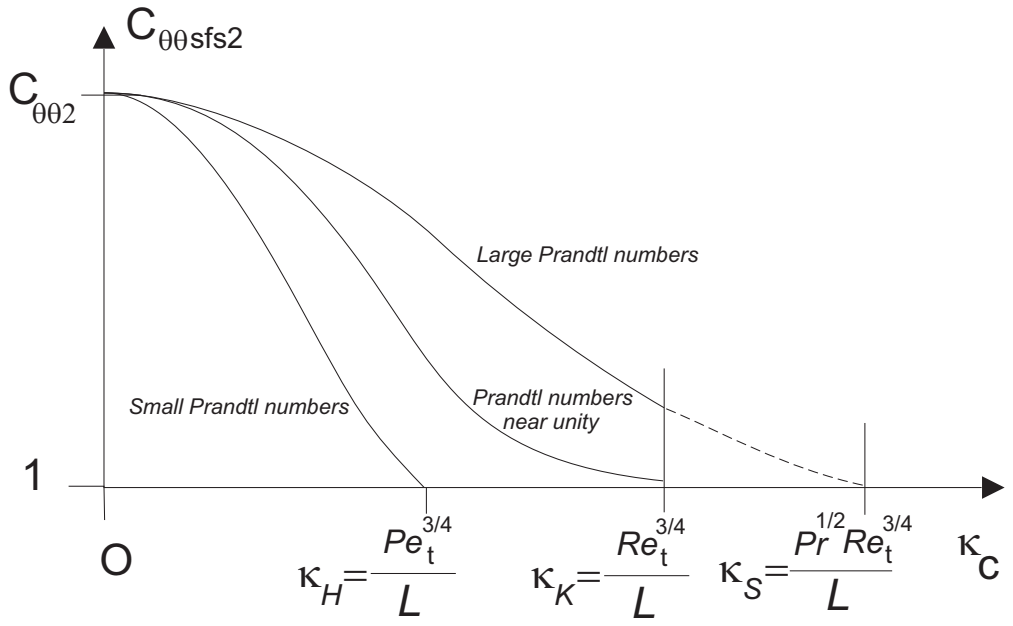

Figure 4: Qualitative sketch of the variation of the coefficient $C_{\epsilon\theta\theta_2}$ versus location of cutoff depending on the Prandtl number ranges.

22. System of equations for passive scalar turbulence

- **Scalar variance**

$$\frac{\partial k_{\theta\,sfs}}{\partial t} + \frac{\partial}{\partial x_k}\left(\bar{u}_k k_{\theta\,sfs}\right) = P_{\theta sfs} + J_\theta - \epsilon_\theta \tag{41}$$

with

$$P_{\theta sfs} = -(\tau_{j\theta})_{sfs}\frac{\partial \bar{\theta}}{\partial x_j} \qquad (\tau_{i\theta})_{sfs} = -c_{\tau_\theta}(\tau_{im})_{sfs}\frac{k_{sfs}}{\epsilon}\frac{\partial \bar{\theta}}{\partial x_m} \tag{42}$$

- **Dissipation-rate of the scalar variance**

$$\frac{\partial \epsilon_\theta}{\partial t} = c_{\epsilon\theta\theta_1\,sfs} P_{\theta sfs}\frac{\epsilon_\theta}{k_{\theta\,sfs}} + c_{\epsilon\theta k_1\,sfs} P_{sfs}\frac{\epsilon_\theta}{k_{sfs}} - c_{\epsilon\theta k_2\,sfs}\frac{\epsilon_\theta \epsilon}{k_{sfs}} - c_{\epsilon\theta\theta_2\,sfs}\frac{\epsilon_\theta^2}{k_{\theta\,sfs}} + J_{\epsilon\theta} \tag{43}$$

23. SET UP OF THE NUMERICAL FLOW SIMULATIONS

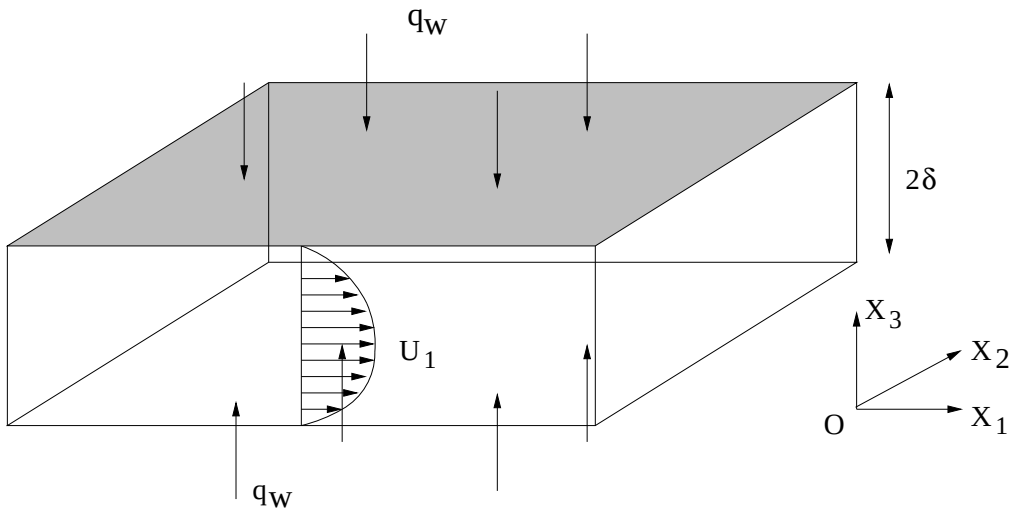

Figure 5: Setup of the numerical channel flow simulations with isoflux thermal boundary conditions. Both walls are heated with a constant flux.

24. NUMERICAL PROCEDURE

- **The dimension of the channel in the streamwise, spanwise and normal directions along the axes x_1, x_2, x_3 are $L_1 = 6.4\delta$, $L_2 = 3.2\delta$ and $L_3 = 2\delta$**
- **Two meshes of medium and coarse grid resolutions**

Case	N_1	N_2	N_3	$N(10^6)$	Δ_1^+	Δ_2^+	Δ_{3c}^+	η_θ
PITM1 (Pr=0.1)	**42**	**21**	**84**	**0.074**	**60**	**60**	**16**	**5.62** η_κ
PITM1 (Pr=1)	**42**	**21**	**84**	**0.074**	**60**	**60**	**16**	η_κ
PITM1 (Pr=10)	**42**	**21**	**128**	**0.112**	**60**	**60**	**16**	**0.316** η_κ
PITM2 (Pr=0.1)	**84**	**42**	**84**	**0.296**	**30**	**30**	**16**	**5.62** η_κ
PITM2 (Pr=1)	**84**	**42**	**84**	**0.296**	**30**	**30**	**16**	η_κ
PITM2 (Pr=10)	**84**	**42**	**128**	**0.452**	**30**	**30**	**16**	**0.316** η_κ

Table 1: grid-points N_i, total number of grid-points N, grid resolution Δ_i^+, x_1, x_2, x_3, Batchelor length-scale η_θ, Kolmogorov length-scale η_κ for the Prandtl numbers $P_r = 0.1$, 1 and 10. PITM simulations $R_\tau = u_\tau\delta/\nu = 395$ (Chaouat and Schiestel, 2021).

25. COMPARISON WITH DNS

- **The dimension of the channel in the streamwise, spanwise and normal directions along the axes x_1, x_2, x_3 are $L_1 = 6.4\delta$, $L_2 = 3.2\delta$ and $L_3 = 2\delta$**
- **Two meshes of refined and highly refined grid resolutions**

Case	N_1	N_2	N_3	$N(10^6)$	Δ_1^+	Δ_2^+	Δ_{3c}^+	η_θ
DNS 1 (Pr=0.1)	**512**	**256**	**256**	**33.55**	**5**	**5**	**2**	**5.62** η_κ
DNS 2 (Pr=1.0)	**512**	**256**	**256**	**33.55**	**5**	**5**	**2**	**1.00** η_κ
DNS 3 (Pr=10)	**1024**	**512**	**1024**	**536.87**	**2.5**	**2.5**	**0.1**	**0.316** η_κ

Table 2: grid-points N_i, total number of grid-points N, grid resolution Δ_i^+, x_1, x_2, x_3, Batchelor length-scale η_θ, Kolmogorov length-scale η_κ for the Prandtl numbers $P_r = 0.1, 1$ and 10. DNS simulations $R_\tau = u_\tau \delta/\nu = 395$ (Chaouat, 2018; Chaouat and Peyret, 2019).

Small Prandtl numbers : $\eta_\theta = (\sigma^3/\epsilon)^{1/4} = \eta_\kappa / P_r^{3/4}$

Prandtl number of unity : $\eta_\theta = \eta_\kappa$

Large Prandtl numbers : $\eta_\theta = (\nu\sigma^2/\epsilon)^{1/4} = \eta_\kappa / P_r^{1/2}$ **and** $N \propto R_t^{9/4} P_r^{3/2}$

26. DNS CODE

- **The numerical DNS code (Chaouat, 2018) is based on the finite volume technique where the mean variables are evaluated at the center of the computational cell whereas the convective and diffusive fluxes are computed at the interfaces surrounding the cell.**
- **The equations are integrated in time using an explicit Runge-Kutta scheme of fourth order accuracy in time $O(\delta t^4)$**
- **The Navier-Stokes equations are solved in space by means of a centered scheme of fourth order accuracy in space $O(\delta x^4)$**
- **The numerical code is highly optimized with message passing interface (MPI) thanks to the compact and explicit formulation of all involved stencils.**
- **List of 6 variables in conservative form solved by the DNS code**
  - ρ, ρu_1, ρu_2, ρu_3, ρE, $\rho\theta$

27. PITM CODE

- **The PITM code (Chaouat, 2005) is also based on the finite volume technique.**
- **The additional transport equations are solved in space by means of an upwind scheme of second order accuracy in space $O(\delta x^2)$**
- **Implicit numerical scheme for the source terms of the transport equations of turbulence**
- **List of 15 variables in conservative form solved by the PITM code**
  - ρ, ρu_1, ρu_2, ρu_3, ρE, $\rho\theta$
  - $\rho(\tau_{11})_{sfs}$, $\rho(\tau_{12})_{sfs}$, $\rho(\tau_{13})_{sfs}$, $\rho(\tau_{22})_{sfs}$, $\rho(\tau_{23})_{sfs}$, $\rho(\tau_{33})_{sfs}$, $\rho\epsilon$
  - $\rho(k_\theta)_{sfs}$, $\rho\epsilon_\theta$

28. Contours of the passive scalar

Figure 6: Contours of the instantaneous passive scalar in the (x_1, x_3) mid-plane illustrating the unsteady character of the scalar field, the detachment of vortex in the normal direction to the wall according to DNS (Chaouat and Peyret, 2019). $P_r = 1$.

29. VELOCITY PROFILES (Coarse and medium grid resolutions)

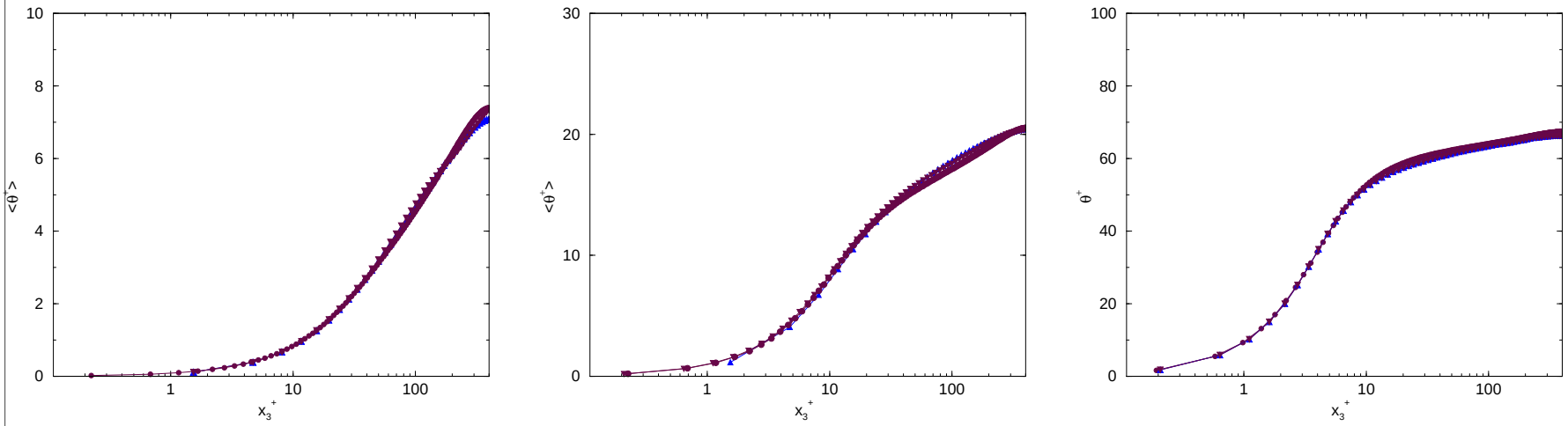

(a) **(b)** **(c)**

Mean scalar field $\langle\theta^+\rangle = \langle\theta\rangle / \theta_\tau$ in logarithmic coordinate versus the wall unit distance for various P_r numbers. PITM1: ▼. PITM2: ▲. DNS : ●. (a) $P_r = 0.1$; (b) $P_r = 1$; (c) $P_r = 10$;

- **Excellent agreement with DNS data (Chaouat and Peyret, 2019).**

30. RMS PROFILES (Coarse grid resolution)

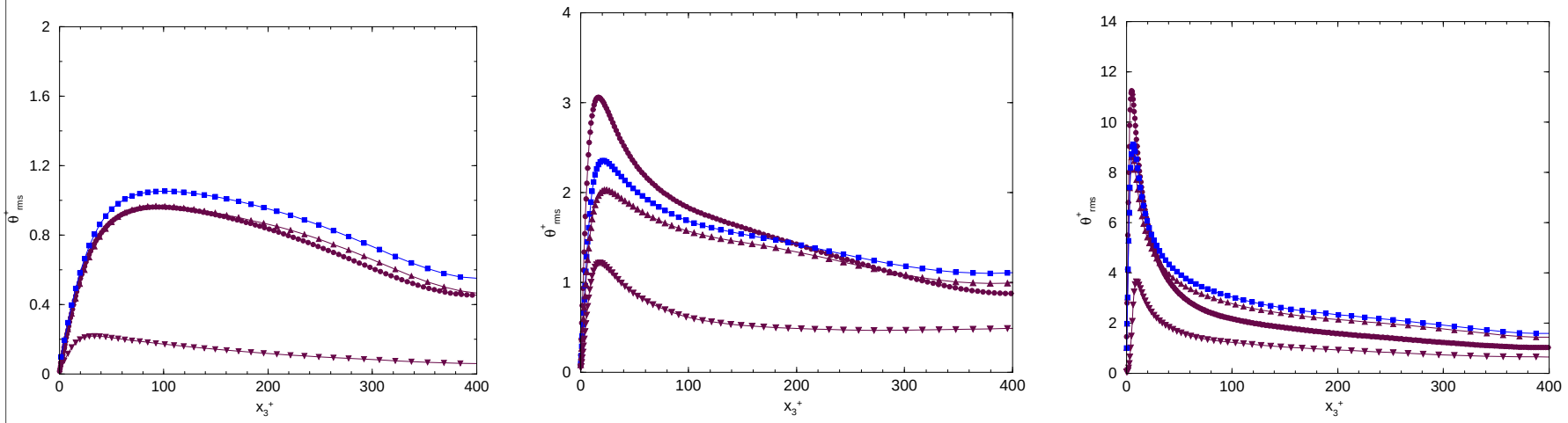

(a) **(b)** **(c)**

Root mean square of the scalar variance $\theta^+_{rms} = \sqrt{\langle \theta'^+ \theta'^+ \rangle} = \sqrt{\langle \theta' \theta' \rangle}/\theta_\tau$ versus the wall distance for various P_r numbers. Subfilter scale : ▼; Resolved scale : ▲. Total scales : ■. (a) $P_r = 0.1$; (b) $P_r = 1$; (c) $P_r = 10$; DNS : ●.

- **Relative good agreement with DNS data (Chaouat and Peyret, 2019).**

31. RMS PROFILES (Medium grid resolution)

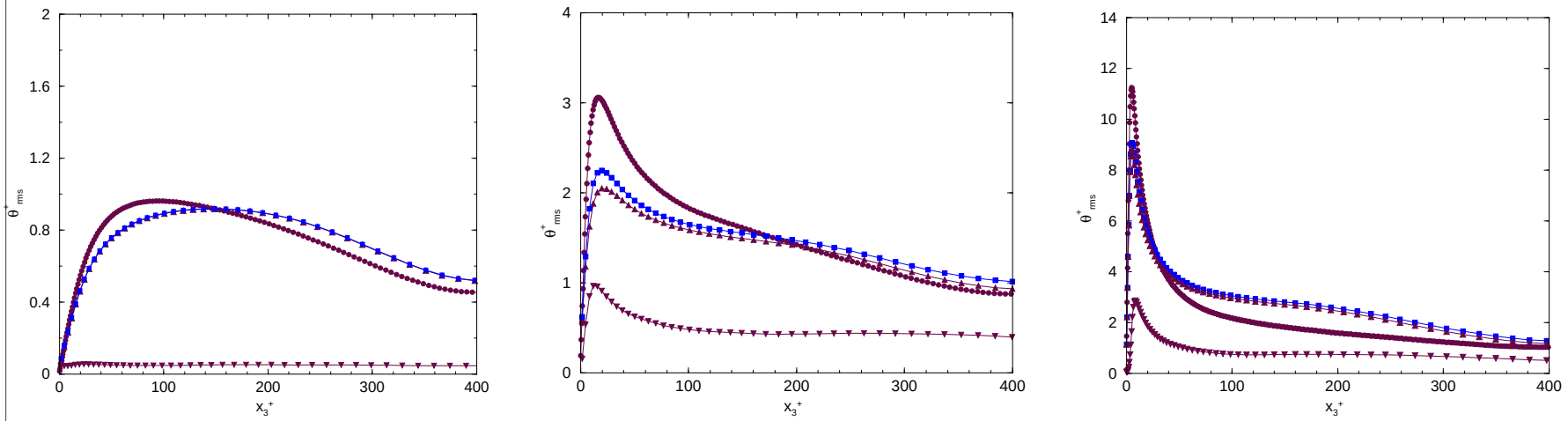

(a) **(b)** **(c)**

Root mean square of the scalar variance $\theta^+_{rms} = \sqrt{\langle \theta'^+ \theta'^+ \rangle} = \sqrt{\langle \theta' \theta' \rangle}/\theta_\tau$ versus the wall distance for various P_r numbers. Subfilter scale : ▼; Resolved scale : ▲. Total scales : ■. (a) $P_r = 0.1$; (b) $P_r = 1$; (c) $P_r = 10$; DNS : ●.

- **Relative good agreement with DNS data (Chaouat and Peyret, 2019).**

ONERA

32. NORMAL TURBULENT HEAT FLUX (coarse grid)

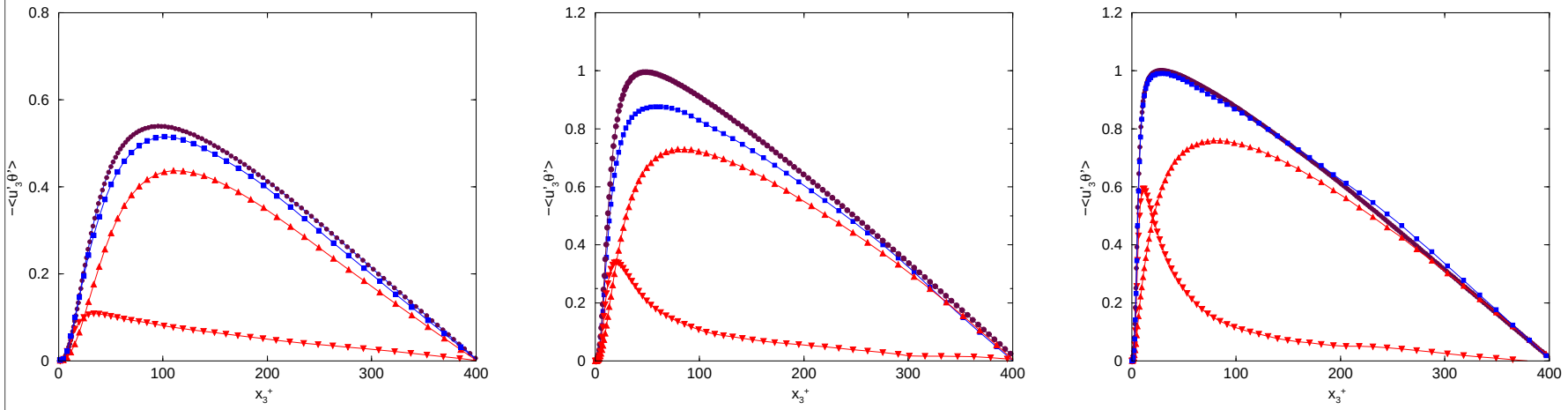

(a) **(b)** **(c)**

Normal turbulent heat fluxes $q_3 = \left\langle u_3'^{+}\theta'^{+}\right\rangle = \left\langle u_3'\theta'\right\rangle / u_\tau\theta_\tau$, versus the wall distance for various Prandtl numbers. (a): P_r=0.1. (b): P_r=1. (c): P_r=10. Subfilter scale : ▼; Resolved scale : ▲; Total scales : ■ . DNS : ●.

- **Excellent agreement is obtained with the DNS data.**
- **Distribution of the SGS/LES part of energy governed by the cutoff wave number κ_c of the grid**

33. NORMAL TURBULENT HEAT FLUX (medium grid)

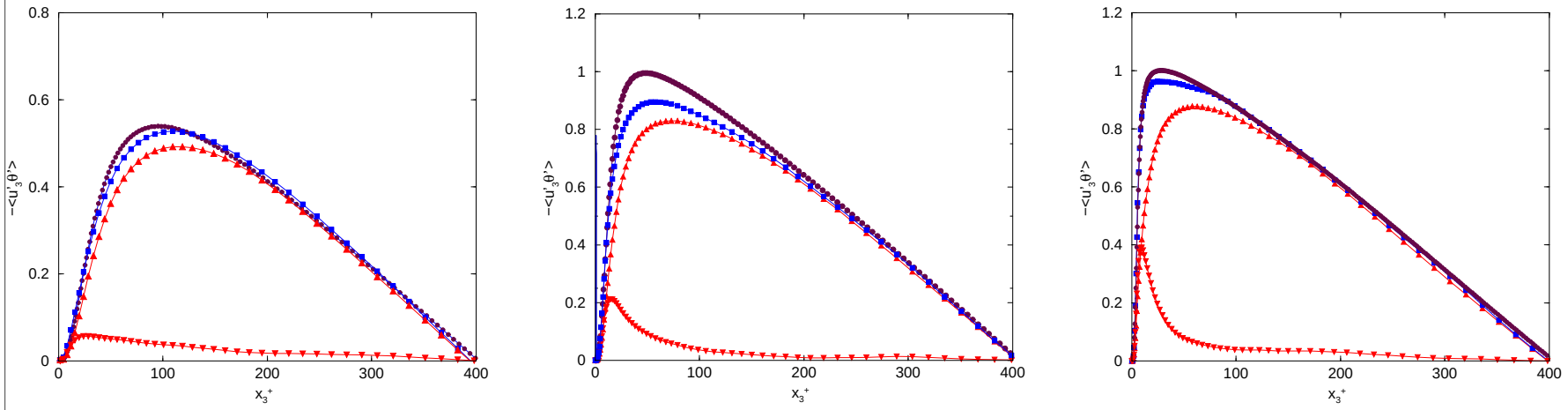

(a) **(b)** **(c)**

Normal turbulent heat fluxes $q_3 = \left\langle u_3'^+ \theta'^+ \right\rangle = \left\langle u_3' \theta' \right\rangle / u_\tau \theta_\tau$, versus the wall distance for various Prandtl numbers. (a): P_r=0.1. (b): P_r=1. (c): P_r=10. Subfilter scale : ▼; Resolved scale : ▲; Total scales : ■ . DNS : ●.

- **Excellent agreement is obtained with the DNS data (Chaouat and Peyret, 2019).**
- **Coarse and Medium grids : decreasing of SGS while increasing of LES according to the cutoff wave number κ_c of the grid**

CONCLUSION

- **The PITM method has been extended for simulating passive scalar fields of turbulent flows**
- **The modeling has been made in the spectral space**
  - **Spectral splitting of the density spectrum**
  - **Partial integration in the spectral space**
- **The equations of the scalar variance k_θ and its dissipation rate ϵ_θ have been devised in the spectral space and transposed to the physical space**
- **The channel flow subjected to constant heat fluxes has been simulated on several meshes of coarse resolution**
  - **The intensity of the RMS fluctuation of the scalar fluctuations was fairly well obtained according to the DNS data**
  - **The profile of the turbulent heat flux was also well reproduced**
- **Practical engineering and geophysical flows will be tackled in the near future using PITM**

References

[1] B. Chaouat. DNS of passive scalar transport fields in turbulent flow at low and high Prandtl numbers. Proc. of 12th Intl ERCOFTAC Symp. on Engng. Turbulence Modelling and Measurements, Montpellier, France, 1–6, 2018.

[2] B. Chaouat and C. Peyret. Investigation of the wall scalar fluctuations effect on passive scalar turbulent fields at several Prandtl numbers by means of direct numerical simulations, Journal of Heat Transfer, ASME, 141(12), 1-12, 2019.

[3] B. Chaouat and R. Schiestel. A new partially integrated transport model for subgrid-scale stresses and dissipation rate for turbulent developing flows. Physics of Fluids, 17(065106):1-19, 2005.

[4] B. Chaouat and R. Schiestel. From single-scale turbulence models to multiple-scale and subgrid-scale models by Fourier transform. Theoretical Computational Fluid Dynamics, 21(3):201229, 2007.

[5] B. Chaouat and R. Schiestel. Extension of the partially Integrated transport modeling method to the simulation of passive scalar fluctuations at various Prandtl numbers. International Journal of Heat and Fluid Flow, 89, 108813, 1-19, 2021.